Slip Ratio Control using Load-side High-resolution Encoder for In-wheel-motor with Reduction Gear

T. Enmei*, H.Fujimoto**, Y. Hori***
The University of Tokyo
5-1-5, Kashiwanoha, Kashiwa, Chiba, 277-8561 Japan
Phone: +81-4-7136-3881
Email: enmei14@hflab.k.u-tokyo.ac.jp*, fujimoto@hflab.k.u-tokyo.ac.jp**, hori@hflab.k.u-tokyo.ac.jp***
D. Gunji
NSK Ltd.,
1-5-50, Kugenumashinmei, Fujisawa, Kanagawa, 251-8501, Japan
Phone: +81-4-7136-3881
Email: gunji-d@NSK.com
K. Omata
Nikon Corporation
471, Nagaodaityou, Sakae, Yokohama, 244-8533 Japan
Phone: +81-4-7136-3881
Email: Kenji.Omata@nikon.com

***Abstract*—Electric vehicles have recently attracted broad attention. Advantage of Electric Vehicles is not only environmental performance but also higher response vehicle motion control when compared to internal combustion engine vehicle. In order to improve motion control performance of Electric Vehicles, applying high-resolution encoders both on a motor side and a wheel side is a good solution. In this paper, the design of the actual vehicle unit for experimental electric vehicle FPEV4-Sawyer is explained. Furthermore, the effectiveness of using high-resolution encoder on vehicle motion control methods is discussed with simulations and experiments of slip ratio control.**

I. Introduction

As the concern for global warming and other environmental problem increases, Electric Vehicles (EVs) are getting attention. EVs are superior to internal combustion vehicles not only in the environmental aspect but also in controllability. Torque generation is accurate and quick, driving force can be estimated, and it is possible to distribute power source within each of the four EV motors[1].

There are many traction control methods based on these advantages[2], [3], [4]. The authors' research group also proposed many EV control methods such as slip ratio control[5] and direct driving force control method[6].

These control methods often assume the use of in-wheel-motor (IWM)[7], [8]. This is because EV with an on-board motor having the drive shaft between the motor and the wheel, are suffered from shaft resonance and it is difficult to detect wheel angle precisely[9]. However, although direct drive IWM performs high controllability, it is expensive and demands a lot of space, which is not suitable for commercial EVs. One simple solution is to mount reduction gear on IWM, but controllability decreases because of gear backlash and elastic deformation.

(a) Experimental electric vehicle FPEV4-Sawyer

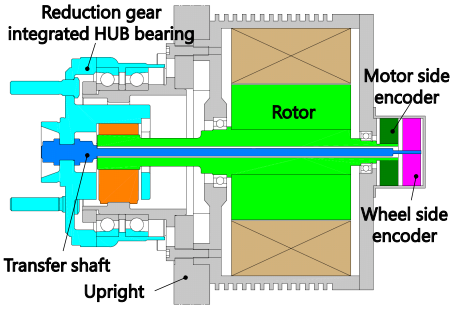

(b) In-wheel motor with high-resolution encoder

Fig. 1. Experimental setup.

Low resolution of wheel resolvers is another problem. Many EV control methods requires the detection of high-order state variables such as wheel angular velocity and acceleration. These information are detected by differentiating the wheel angle. However, wheel resolvers' resolution is around 10 bit and this is not enough to obtain high order information[10], [11], [12], [13]

TABLE I
SPECIFICATIONS OF EXPERIMENTAL VEHICLE.

Parameter	Value
Vehicle mass M	1183 kg
Wheel inertia J_ω	2.25 kgm^2
Tire radius r	0.574 m

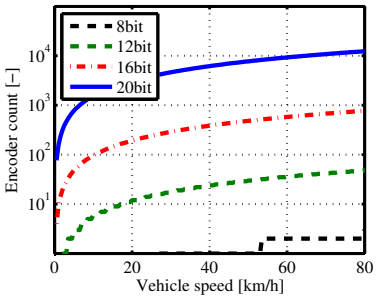

Fig. 2. Encoder count per sampling period.

To solve these problems, the authors propose to mount high-resolution optical encoder on the load-side of IWMs and take wheel angle directly. Recently, optical encoders are widely used in industrial fields and their cost is decreasing. Their resolution is now over 20 bit and resistance to impact is high enough for the use in industrial robots. Therefore, application to IWM is possible.

In this paper, we propose a structure of IWM which can mount high-resolution encoder on the load-side of the reduction gear and the required resolution for EV motion controls is discussed. The validity of the proposed method is presented by simulations and experiment of slip ratio control.

II. Experimental setup

A. Experimental vehicle

Experimental vehicle is FPEV4-Sawyer, manufactured by our research group. Fig. 1(a) is its appearance and Table I shows its specifications. The prototype of FPEV4-Sawyer is commercial EV "i-MiEV", produced by Mitsubishi Motors Corporation, and the control method studied in this paper can be widely applied to general commercial EV.

B. IWM with load-side high-resolution encoder

The authors' research group developed IWM with reduction gear and load-side high-resolution encoder. This motor is mounted on FPEV4-Sawyer and some experiments are conducted in this paper. It has a planetary gear in the hub bearing and can generate large input in spite of its size.

The most important feature of this motor is that it has high-resolution encoders both on the motor-side (input side of the reduction gear) and on the load-side (output side of the reduction gear).Conventional direct drive in-wheel-motor equips the motor-side encoder only. However, there is torsion or nonlinearity between the motor-side and load-side of reduction gears. Therefore, it is not enough to obtain precise wheel angular information.

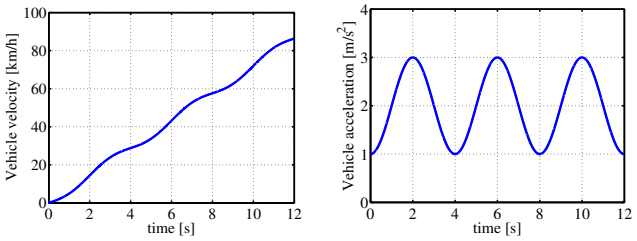

(a) V (b) a

Fig. 3. Driving pattern (simulation).

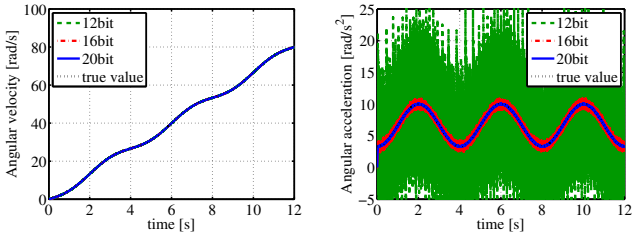

(a) ω (b) $\dot{\omega}$

Fig. 4. High order state variables with different resolutions (simulation).

The authors' research group proposed a structure to solve this problem in[14] and applied to IWM in this paper. Fig. 1(b) shows cross section of our experimental IWM. There is an output shaft between the load and the load-side encoder through the hollow motor, and the motor-side encoder and the load-side encoder are equipped side by side. This optical encoder, whose resolution is 20 bit, is manufactured by Nikon and is often used for industrial robots. The mechanical resonance frequency of the output shaft is sufficiently high because the shaft has high rigidity and the moment of inertia of the load-side encoder is very small.

III. Quantization noise and encoder resolution

The relationship between quantization noise and encoder resolution is discussed in this section. When angular velocity or acceleration is obtained by pseudo differentiation, there are noise attributes to quantization error. In this section, M-method is used to count encoder pulse. M-method gives accurate detection of high-order state variable with high resolution and sampling frequency. Here, by assuming the sampling period of 1 ms, the required encoder resolution is discussed.

A. Encoder count per sampling period

Optical encoders whose resolution is n bit can count N_c pulses, calculated by (1), per one sampling period.

$$N_c = \left\lfloor \frac{2^{n-1} V T_s}{\pi r} \right\rfloor \tag{1}$$

T_s, V and r respectively means sampling period, vehicle speed and tire radius. The symbol '$\lfloor\cdot\rfloor$' in(1) means floor function, maps real number to the largest previous integer.

Fig. 2 plots the relationship between the vehicle speed and the encoder count per sampling period when the resolution is

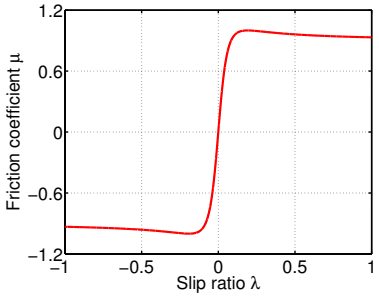

Fig. 5. μ-λ curve.

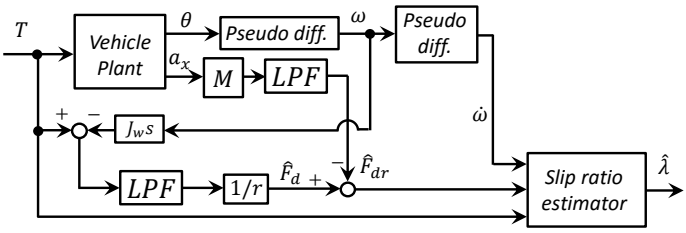

Fig. 6. Block diagram of SRE.

8, 12, 16 and 20 bit. The sampling frequency is assumed to be 1 kHz. Current petrol vehicles use 8 bit position sensors, which is too rough for high sampling rate of EV. Even if the encoder has a resolution of 12 bit, only a few pulses can be obtained in the low speed drive. This means 12 bit resolvers are not enough when we suppose the case such as start on the low friction road surface. On the other hand, with the resolution of 20 bit, more than 100 pulses can be taken even in start motion.

B. Detection of angular velocity and acceleration

High order state variables such as angular velocity ω and acceleration $\dot{\omega}$ can be obtained by pseudo-differential of encoder output θ. (2) is the transfer function of the pseudo-diff.

$$\omega = \frac{s}{1+\tau_d s}\theta, \quad \dot{\omega} = \left(\frac{s}{1+\tau_d s}\right)^2 \theta \tag{2}$$

τ_d decides the cutoff frequency of the LPF. There is a tradeoff between quantization noise suppression and phase delay. As τ_d gets larger, the quantization noise becomes smaller and the phase delay increases.

A simulation of wheel angular velocity and acceleration detection is conducted about the resolution of 12 bit, 16 bit and 20 bit in the case that τ_d is $1/40\pi$ seconds. Driving pattern is shown on Fig. 3. Here the wheel slip is assumed to be zero. The acceleration pattern is a sinusoidal signal whose amplitude is 1 m/s^2, frequency is 0.25 Hz, and offset is 2 m/s^2.

Fig. 4 is the simulation result. Fig. 4(a) and Fig. 4(b) shows the detected angular velocity and acceleration respectively. About the rotation speed detection, each case shows good accuracy. However, in wheel acceleration detection, according to encoder resolution, there is quantization noise. Conventional 12 bit encoder has large noise ripple and its detection error is

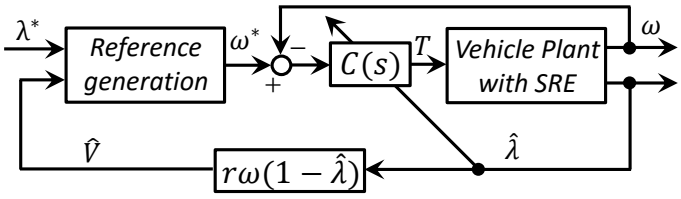

Fig. 7. Block diagram of Slip ratio control.

over 10 rad/s^2 unacceptable for motion control. On the other hands, in the case with 20 bit encoder, detection error is under 0.2 rad/s^2 and accurate enough for control purposes.

From these simulation results, resolution of 20 bit is required for wheel acceleration detection. Thus, the tradeoff between phase delay and noise can be solved by the use of high-resolution encoder. Since the road surface changes occur as step disturbances for slip ratio, reducing the phase delay is critical.

IV. Slip ratio estimation and control

A. Slip ratio estimation without vehicle speed detection

There is slip on wheels generating driving force. Slip ratio is the physical quantity indicating the amount of the slip. Slip ratio λ is defined as (3) by using vehicle speed V and wheel velocity ω.

$$\lambda_{ij} = \frac{V_{\omega ij} - V}{\max(V_{\omega ij}, V, \epsilon)} \tag{3}$$

Subscript i is "f" or "r", which means "front" or "rear". Subscript j is "l" or "r", which means "left" or "right". ϵ is the small constant to avoid zero denominator. In case of acceleration, (3) can be expressed as (4).

$$\lambda_{ij} = \frac{r\omega_{ij} - V}{r\omega_{ij}} \tag{4}$$

r means wheel radius. In this paper, since only accelerating cases are considered, (4) is used as the definition of the slip ratio.

Fig. 5 shows the relation of slip ratio and friction coefficient determining the driving force between the wheel and the ground. Measurement of slip ratio greatly contributes to safety. Vehicle speed V is often detected by the non-driven wheel. However, 4 wheel drive IWM EVs do not have non-driven wheels and cannot measure vehicle speed. Since acceleration sensors have sensor offsets, the vehicle speed cannot be detected by integration. Optical speed sensors are expensive and not suitable for commercial vehicles.

Therefore, in[5], the authors' research group proposed the slip ratio estimation (SRE) method without vehicle speed detection.

Following (5) can be obtained by differentiating (4).

$$\dot{\lambda}_{ij} = \frac{r\omega_{ij}\dot{\omega}_{ij}(1-\lambda_{ij}) - \omega_{ij}\dot{V}}{r\omega_{ij}^2} \tag{5}$$

TABLE II
SIMULATION CONDITIONS.

Parameter	Value
Vehicle mass M	1300 kg
Sampling frequency	1 kHz
Input torque T	300 Nm
Encoder resolution	12, 20 bit
Cutoff frequency	12, 240 Hz

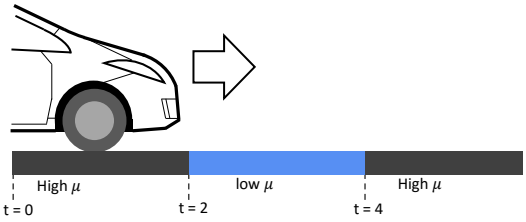

Fig. 8. The road condition of the simulation.

Here, the motion equation of the wheels is (6).

$$J_{\omega ij}\dot{\omega}_{ij} = T_{ij} - rF_{dij} \tag{6}$$

T, F_d, J_ω are input torque, driving force, and wheel inertia respectively. The translational motion equation of the vehicle is (7).

$$M\dot{V} = \sum_{i=f,r}\sum_{j=l,r} F_{dij} - F_{dr} \tag{7}$$

M and F_{dr} are vehicle mass and driving resistance respectively. In order to remove V, (6) and (7) are rearranged into (5). Thus, (8) can be obtained.

$$\dot{\lambda}_{ij} = -\frac{\dot{\omega}_{ij}}{\omega_{ij}}\lambda_{ij} + \left(1 + \frac{1}{r^2M}\sum_{i=f,r}\sum_{j=l,r} J_{\omega ij}\right)\frac{\dot{\omega}_{ij}}{\omega_{ij}} - \frac{1}{r^2M\omega_{ij}}\sum_{i=f,r}\sum_{j=l,r} T_{ij} + \frac{F_{dr}}{rM\omega_{ij}} \tag{8}$$

Since driving resistance F_{dr} cannot be measured directly by any sensors, F_{dr} should be estimated. By adopting disturbance observer with (7), F_{dr} can be estimated as (9).

$$\hat{F}_{dr} = \sum_{i=f,r}\sum_{j=l,r} \hat{F}_{dij} - M\dot{V} \tag{9}$$

Here, $\hat{F}_{dr}$ and $\hat{F}_{dij}$ are estimated driving resistance and driving force of each wheel respectively. In order to measure $\dot{V}$, acceleration sensor value is used. Therefore, estimated slip ratio $\hat{\lambda}$ can be obtained as (10).

$$\dot{\hat{\lambda}}_{ij} = -\frac{\dot{\omega}_{ij}}{\omega_{ij}}\hat{\lambda}_{ij} + \left(1 + \frac{1}{r^2M}\sum_{i=f,r}\sum_{j=l,r} J_{\omega ij}\right)\frac{\dot{\omega}_{ij}}{\omega_{ij}} - \frac{1}{r^2M\omega_{ij}}\sum_{i=f,r}\sum_{j=l,r} T_{ij} + \frac{\hat{F}_{dr}}{rM\omega_{ij}} \tag{10}$$

Fig. 6 shows the block diagram of SRE.

Estimation error of SRE is defined as (11).

$$e(t) = \lambda - \hat{\lambda} \tag{11}$$

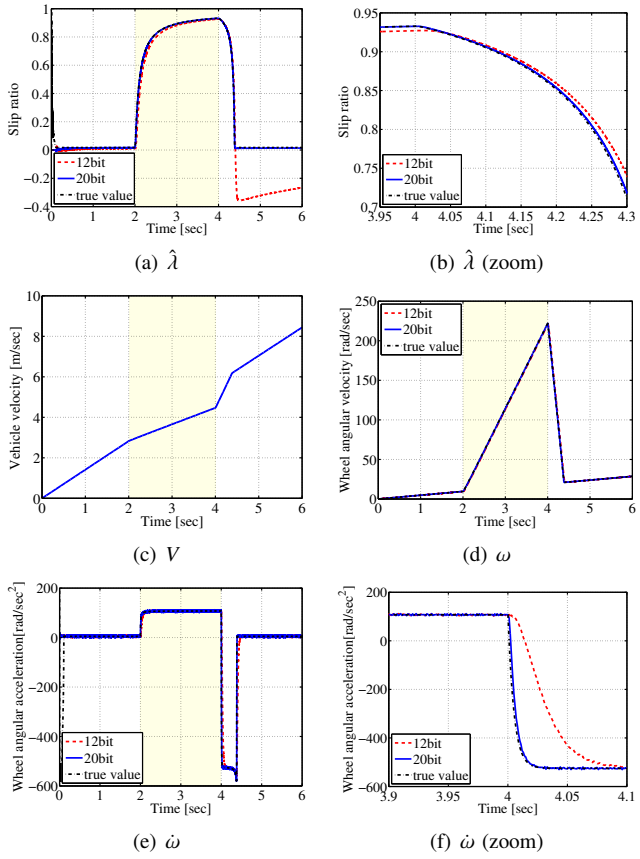

(a) $\hat{\lambda}$ (b) $\hat{\lambda}$ (zoom)

(c) V (d) ω

(e) $\dot{\omega}$ (f) $\dot{\omega}$ (zoom)

Fig. 9. Simulation results.

Following relation about convergence can be obtained from (10) and (11).

$$\frac{d}{dt}e(t) = -\frac{\dot{\omega}}{\omega}e(t) \tag{12}$$

When $\frac{\dot{\omega}}{\omega} > 0$, estimation error converges to zero.

In order to adopt SRE, $\dot{\omega}$ must be detected accurately with small phase delay. In this paper, the authors proposed to use high-resolution encoder and obtained accurate high-order state variables.

B. Slip ratio control based on SRE

In[5], slip ratio control (SRC) method using wheel speed minor loop is proposed. Fig. 7 is its block diagram. Here, $C(s)$ is minor loop angular velocity controller. In this paper, SRE is used for λ detection.

Vehicle speed V can be calculated as (13).

$$\hat{V} = r\omega(1 - \hat{\lambda}) \tag{13}$$

To achieve desired slip ratio λ^*, wheel angular velocity ω should be following ω^*.

$$\omega^* = \frac{\hat{V}}{r(1 - \lambda^*)} \tag{14}$$

Therefore, ω is controlled by wheel speed minor loop as shown on Fig. 7.

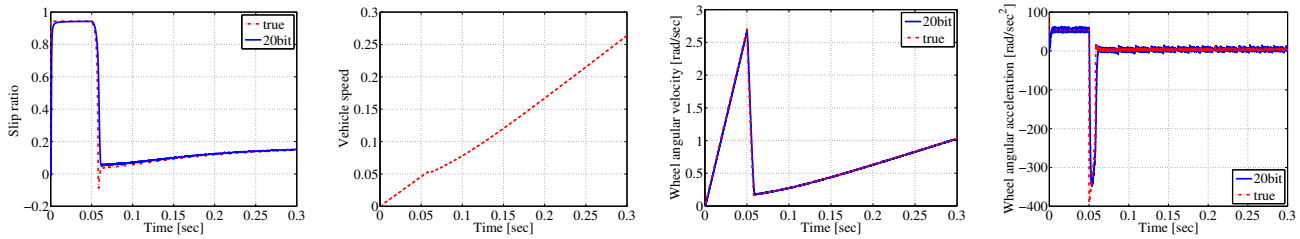

(a) $\hat{\lambda}$ (b) V (c) ω (d) $\dot{\omega}$

Fig. 10. Slip ratio control (simulation, 20bit).

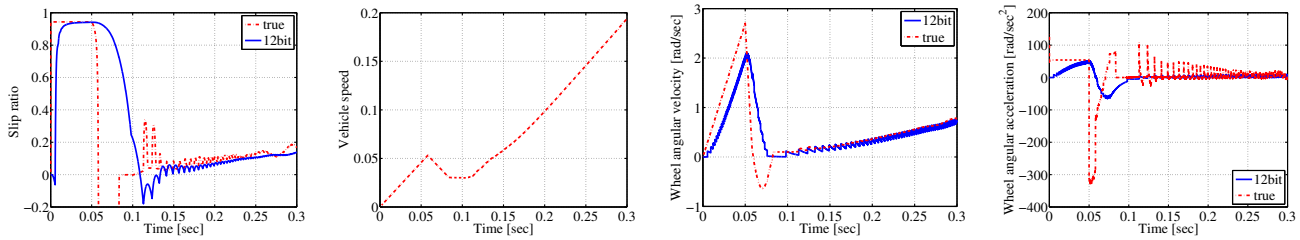

(a) $\hat{\lambda}$ (b) V (c) ω (d) $\dot{\omega}$

Fig. 11. Slip ratio control (simulation, 12bit).

The transfer function of T to ω is (15).

$$\frac{\omega}{T} = \frac{1}{(J_\omega + r^2 M(1-\lambda))s} \tag{15}$$

Since (15) changes according to λ, variable gain controller is used and designed by pole placement.

V. Simulation

A. Simulation of slip ratio estimation

The relation between estimation accuracy of SRE and encoder resolution is discussed by means of simulation. The road condition is assumed to be high μ road and low μ road from $t = 2$ to $t = 4$ as shown on Fig. 8. Table II shows the simulation conditions. Magic formula is used as a tire model[15]. The input torque is 300 Nm constant. Angular velocity and acceleration are calculated by pseudo-differential and their cut-off frequencies are decided so that their quantization noise become similar extent.

Fig. 9 shows the simulation result. With 12 bit encoder, estimation error of $\hat{\lambda}$ does not converges to 0 in adhesion phase after the slip in Fig. 9(a). This is because the phase delay of the estimator expands like Fig. 9(b) while $\frac{\dot{\omega}}{\omega}$ stays negative. On the other hand, with 20 bit high-resolution encoder, high-order state variables can be detected with smaller phase delay as shown on Fig. 9(d), (e), and(f). Therefore, estimation error becomes much smaller than 12 bit case even though $\frac{\dot{\omega}}{\omega}$ becomes negative in adhesion phase.

B. Simulation of slip ratio control

Simulation of slip ratio control is conducted with both 12 bit and 20 bit encoders. The road condition is assumed to be low μ road throughout the simulation. Constant 300 torque Nm is applied from $t = 0$ to $t = 0.05$ and tire slip is caused. After that, slip ratio is controlled so that λ becomes 0.2 and its controller is designed so that the poles are placed on 5 Hz.

Fig. 10 and Fig. 11 are the simulation result with 20 bit and 12 bit encoder respectively. With 12 bit encoder, slip ratio response of true value is vibrating and has large overshoot. Large estimation error declines controllability. On the other hand, 20 bit encoder can achieve good estimation and control.

VI. Experiment

An experiment of SRE with high resolution encoder was conducted with low μ sheet. After the experimental vehicle starts moving on the low μ sheet and a wheel slip occurs, it enters high μ road and wheel adheres to road.

By decimating the 20 bit load side encoder signal, 12 bit wheel resolver is emulated and they are compared. Experimental condition is shown on Table III. True value of slip ratio is taken by the use of the wheel encoder on the front tire. Since the wheel angle obtained in the experiment includes mechanical vibration of the motor and other kind of noise, the cutoff frequency of the pseudo differential cannot be raised as high as that in simulation.

Fig. 12 is the experimental result. The cutoff frequency of the pseudo differential for 20 bit encoder is decided based on noise ripple of acceleration detected 12 bit resolver. As shown on fig Fig. 12(a) and (b) similar result in Fig. 9(a) and (b) can be obtained. With the resolution of 12 bit, large estimation error occurs in the adhesive phase whereas does not with 20bit encoder.

VII. Conclusion

Conventionally, in order to obtain EV wheel angle information, motor-side encoders or resolvers whose resolution was around 10 bit were used. However, this measurement

TABLE III
EXPERIMENTAL CONDITIONS.

Parameter	Value
Sampling period	166 μs
Encoder resolution	12, 20 bit
Cutoff frequency	12, 72 Hz
Discretization frequency	1 kHz

accuracy is not enough to make full use of EV motors' good controllability because vehicle motion control often requires detection of high order state variables.

In this paper, we proposed to apply load-side high-resolution encoders to IWM with reduction gear and presented its structure. The required resolution was discussed and that of 20 bit is accurate enough for EV. The validity of proposed method was shown through SRE and SRC simulations and SRE experiments was conducted.

Future work consists of slip ratio control experiments and backlash compensation methods.

ACKNOWLEDGMENT

This research was partly supported by the Ministry of Education, Culture, Sports, Science and Technology grant (numbers 26249061). In addition, attendance to this conference is supported by Research Foundation for the Electrotechnology of Chubu. Finally, the authors would like to express their deepest appreciation to Toyo Denki Seizo K.K for providing the inverter and the motor used in these experiments.

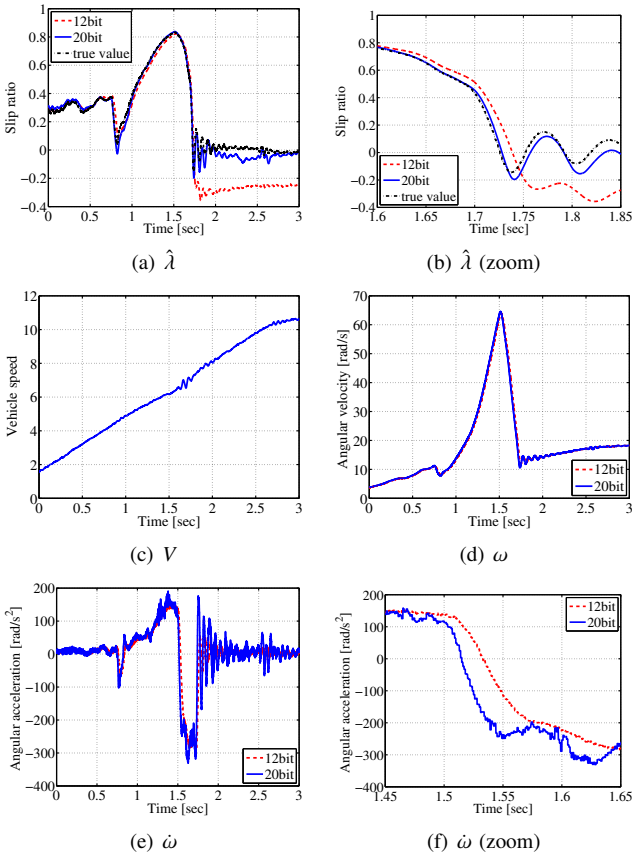

(a) $\hat{\lambda}$ (b) $\hat{\lambda}$ (zoom)

(c) V (d) ω

(e) $\dot{\omega}$ (f) $\dot{\omega}$ (zoom)

Fig. 12. Experimental results.

REFERENCES

[1] Y. Hori, "Future vehicle driven by electricity and control - Research on four-wheel-motored "UOT Electric March II"," *IEEE Transactions on Industrial Electronics*, vol. 51, no. 5, pp. 954–962, 2004.

[2] H. Zhou and Z. Liu, "Vehicle yaw stability-control system design based on sliding mode and backstepping control approach," *IEEE Transactions on Vehicular Technology*, vol. 59, no. 7, pp. 3674–3678, 2010.

[3] W.-P. Chiang, D. Yin, M. Omae, and H. Shimizu, "Integrated Slip-Based Torque Control of Antilock Braking System for In-Wheel Motor Electric Vehicle," *IEEJ Journal of Industry Applications*, vol. 3, no. 4, pp. 318–327, 2014.

[4] G. Erdogan, "Adaptive Vibration Cancellation for Tire-Road Friction Coefficient Estimation on Winter Maintenance Vehicles," *IEEE Trans. Control Syst. Technol.*, vol. 18, no. 5, pp. 1023–1032, 2010.

[5] K. Fujii and H. Fujimoto, "Traction control based on slip ratio estimation without detecting vehicle speed for electric vehicle," in *PCC-NAGOYA 2007*, 2007, pp. 688–693.

[6] M. Yoshimura and H. Fujimoto, "Driving Torque Control Method for Electric Vehicle with In-Wheel Motors," *IEEJ Transactions on Industry Applications*, vol. 131, no. 5, pp. 721–728, 2011.

[7] H. Fukudome, "Reduction of vehicle longitudinal vibration by in-wheel motors," in *2015 JSAE Congress (Autumn)*, 2015, pp. 448–453.

[8] S. Ohno and K. Ito, "Unsprung vibration control for in-wheel-motor," in *Proc. of JSAE Annual Congress (Autumn)*, 2014, pp. 21–24. [Online]. Available: Lib scanned

[9] H. Sumiya and H. Fujimoto, "Driving Force Control Method Using Suppression Control of Driving-shaft Vibration for Electric Vehicle with On-board Motor," in *Proc. IEEJ Industory Apprications Society Conf*, no. 106, 2012, pp. 115–120.

[10] T. Enmei, H. Fujimoto, and Y. Hori, "Slip Ratio Estimation for In-wheel Motors with Reduction Gears using Load-Side High Resolution Encoders," in *2016 IEE-Japan Industry Applications Society Conference*, vol. 4, 2016, pp. 91–94.

[11] M. Kanematsu, H. Zhu, T. Miyajima, H. Fujimoto, and Y. Hori, "Angular Acceleration Detection Method by Ultra-high Resolution Encoder with Hybrid Sampling Time for Automotive Motor Application," in *Proc. IEEJ technical meeting on Rotating Machinery, Linear Drive, and Home and Consumer Appliances*, no. RM-13-072, LD-13-082, HCA-13-048, 2013, pp. 37–42.

[12] M. Nandayapa, C. Mitsantisuk, and K. Ohishi, "High Performance Velocity Estimation for Controllers with Short Processing Time by FPGA," *IEEJ Journal of Industry Applications*, vol. 1, no. 1, pp. 55–61, 2012.

[13] T. Tsuji, T. Hashimoto, S. Member, H. Kobayashi, M. Mizuochi, and K. Ohnishi, "A Wide-Range Velocity Measurement Method for Motion Control," *IEEE Transactions on Industrial Electronics*, vol. 56, no. 2, pp. 510–519, 2009.

[14] S. Yamada, K. Inukai, H. Fujimoto, K. Omata, Y. Takeda, and S. Makinouchi, "Joint torque control for two-inertia system with encoders on drive and load sides," *Proceeding - 2015 IEEE International Conference on Industrial Informatics, INDIN 2015*, vol. 1, pp. 396–401, 2015.

[15] E. H.B.Pacejka, "the Magic Formula Tyre Model ," *Proc. 1st International Colloquium on Tyre Models for Vehicle Dynamics Analysis*, vol. 131, 1991.